Carbon Trends 4 (2021) 100046

Contents lists available at ScienceDirect

Carbon Trends

journal homepage: www.elsevier.com/locate/cartre

A combined experimental and computational study of the Cu/C (sp^2) interface

Xin You[a], Rui Bao[a,b,c], Liangqi Zhang[a], Xiao Huang[a], Jianhong Yi[a,b,*], Xianghui Hou[c,**], Sanliang Ling[c]

[a] Faculty of Materials Science and Engineering, Kunming University of Science and Technology, Kunming 650093, China
[b] State Key Laboratory of Powder Metallurgy, Central South University, Changsha 410083, China
[c] Advanced Materials Research Group, Faculty of Engineering, University of Nottingham, University Park, Nottingham NG7 2RD, UK

ARTICLE INFO

Article history:
Received 15 December 2020
Revised 16 March 2021
Accepted 16 March 2021

Keywords:
Nano sp^2-Carbon material
Cu/Cu_2O/GR interface
DFT calculation
Electrical structures
Work function

ABSTRACT

Interface optimization is the most important and eternal research issue in preparation of the metal matrix composites (MMCs). For nano sp^2-carbon material (NSCM)/metal composites, interfacial precipitates are usually formed intentionally or unintentionally, however, the effect of the interface structure and precipitates on the electron transport properties is still unclear, which is especially important for Cu-based material due to the electronic and electrical applications. In this paper, a series of interface models were constructed based on the transmission electron microscopy (TEM) observation of NSCM/Cu composite and calculated through density functional theory (DFT). The geometric structure, interfacial charge transfer, work function, Bader charges, electron differential density distribution and electronic density of states of Cu/graphene (GR), Cu_2O/GR, Cu/Cu_2O and Cu/Cu_2O/GR interfaces were discussed in detail, we conclude that the Cu_2O precipitates at the Cu/GR interface can reduce the average distance and increase the binding energy between Cu and GR. Besides, the formation of Cu_2O can improve the electronic transport between Cu_2O and copper instead of the weak binding of the Cu and graphene, but Schottky barrier at the interface remains an obstacle need to be overcome. The results can provide reference for the interface design of MMCs and the improvement of the composite properties.

1. Introduction

Nano sp^2-Carbon Material (NSCM), which is known as carbon dominant carbonaceous material [1], has inherent unit structural characteristics of conjugated network, the topological structure of the conjugated carbon-carbon double bond and the consequent excellent performance in mobile devices, aerospace and new energy material application areas [2–4]. NSCM like graphene, graphene oxide, reduced graphene oxide and carbon nanotube (CNT), very recently, are widely used as reinforcements of the MMCs, such as Cu, Ti, Al, Mg and Ni etc. matrixes [5–9]. NSCM/copper (Cu) composites, as one of the most important MMCs, have received more attention for their latent value of scientific research and industrial application owing to their excellent mechanical prosperity, electrical and thermal properties and high temperature stability simultaneously.

For NSCM/Cu composites, the biggest challenge to address is the weak interface binding, which is caused by the natural quality of non-wettability and non-solubility between the carbon and metal matrix, hence no stable phase can be formed in the Cu–C composite [10–12]. As a result, a tight and dense interface is difficult to achieve by traditional densification process. This weak binding and lattice mismatch between sp^2-C and Cu may lead to interface decoupling, and following deteriorate the mechanical, electrical and thermal properties of the NSCM/Cu composites due to the pore and vacancy formed at the interface.

To enhance the interface binding, lots of strategies have been exploited and developed, formation of transition phases like Cu_2O

* Corresponding authors at: Faculty of Materials Science and Engineering, Kunming University of Science and Technology, Kunming 650093, China.
** Corresponding authors at: Advanced Materials Research Group, Faculty of Engineering, University of Nottingham, University Park, Nottingham NG7 2RD, UK.
E-mail addresses: baorui@kmust.edu.cn (R. Bao), yijianhong@kmust.edu.cn (J. Yi), xianghui.hou@nottingham.ac.uk (X. Hou).

https://doi.org/10.1016/j.cartre.2021.100046

[13], TiC [14], Cr_3C_2 [15] and Mo_2C [16] nanoparticles etc. at the surface is one of the most commonly used method. Cu–O bond is discovered to provide strong interfacial bonding between the Cu matrix and carbon reinforcements, which can be attributed to enhanced chemical interactions between O and Cu/C at the interface. Hence, functionalization of sp^2-carbon with oxygen-containing groups and *in-situ* formation of Cu_2O nanocrystals at the interface are expected to prepare stable sp^2-Cu/C composites [17,18].

Unfortunately, simply improving the mechanical properties at the expense of other properties, e.g. electrical or thermal conduction, will greatly limit the application prospects and scope of this composite, because the sp^2–Cu/C composites are also excellent candidates for electrical and thermal management applications due to the high electrical and thermal conductivity of Cu (58.5×10^6 S/m of pure Cu at 20 °C, ~400 W/m K) as well as sp^2 carbon (10^5–10^6 S/m, 3000–6000 W/m K of CNT) [19,20]. But the clear influence of the sp^2–Cu/C interface on electronic transport is still not fully understood, because it is difficult to observe the atomistic structure of the interface in the obtained samples (even under in-situ transmission electron microscopy analysis), even not to mention the understanding on the mechanism of the electron transfer at the interface.

Hence, to better understand the structural and electrical properties of sp^2–Cu/C composites and to develop new strategies to improve their mechanical, electronic and thermal transport properties, in this work, we prepared CNT/Cu composite with nano-Cu_2O transition phase formed at first, then based on our high-resolution transmission electron microscopy (HRTEM) analysis, the interface structure as well as Cu_2O precipitates in interfacial bonding and the electronic structures of Cu/C composite were studied by accurate density functional theory (DFT) calculations. Geometric structure, interfacial charge transfer, work function, electronic density of states and electron differential density distribution of the Cu/C interface were investigated carefully. Then the electron transfer at the interfaces was further discussed in detail.

2. Methods and models

2.1. Experimental methods

Multiwalled-CNT dispersion (MWCNT: ID: 5–20 nm, OD: 30–50 nm, Length: 1–2 mm, CNT content: 10.3 wt% composition: non-ionic surfactant) was purchased from Chengdu Organic Chemistry Co. Ltd., China. Dendritic copper powder (99.9%, Shanghai Naiou Nano Technology Co. Ltd., Shanghai, China) produced by electrolysis was employed in this study. Ball milling was used to change the as-received Cu powder into flaky powder at a rotating speed of 300 r/min for 10 h in a one-way manner (with ethanol medium), stainless steel balls and jar were employed, and the ball-to-powder ratio was 10:1. Then the Cu flaked powders was mixed with CNT reinforcement by low energy ball milling for 2 h (150 r/min). Then this composite powder was annealed at 573 K for 6 h under an Ar-5%H_2 flow to remove the oxide introduced during ball milling. After that, 0.4 wt% CNT-Cu composite powders were consolidated by spark plasma sintering (LABOX-650F furnace). The compact powders were sintered at 1073 K for 10 min under an axial pressure of 50 MPa in a high vacuum chamber. The size of the bulk samples was 20 mm in diameter and ~3 mm in thickness. The morphology of the interface microstructure of the bulk composites were observed by transmission electron microscopy (TEM, Tecnai G2 TF30 S-Twin, FEI, Hillsboro, OR, USA).

2.2. Computational methods and models

All first-principle calculations were carried out using the Vienna Ab initio Simulation Package (VASP) [21] based on density functional theory (DFT) using plane-wave basis sets. To treat the exchange-correlation interaction of electrons, we chose the Perdew–Burke–Ernzerhof (PBE) functional within the generalized gradient approximation (GGA). The electron-ion interactions were described by the projector augmented wave (PAW) potentials. A dipole correction was applied to avoid spurious interactions between periodic images of the slab [22]. To have a better description of the long-range van der Waals (vdW) interactions between different slabs, the semi-empirical dispersion-corrected DFT-D3 scheme proposed by Moellmann and Grimme was adopted [23]. The energy cutoff for plane-wave basis was set at 400 eV. We applied the GGA+U correction on the Cu (d) states for electronic structure calculations involving Cu_2O. We chose a U_{eff} = 7.0 eV for Cu atoms of Cu_2O following previous literature [24]. A convergence criterion of 10^{-4} eV for the total energy and 0.01 eV/Å for the force were adopted for the self-consistent calculation and the geometry optimization, respectively. During the geometry optimization of each interface, no atomic layers were fixed and all atoms were allowed to relax in order to maximally release the strain due to the lattice mismatches between different materials. All the models in this paper are built by the VESTA software [25].

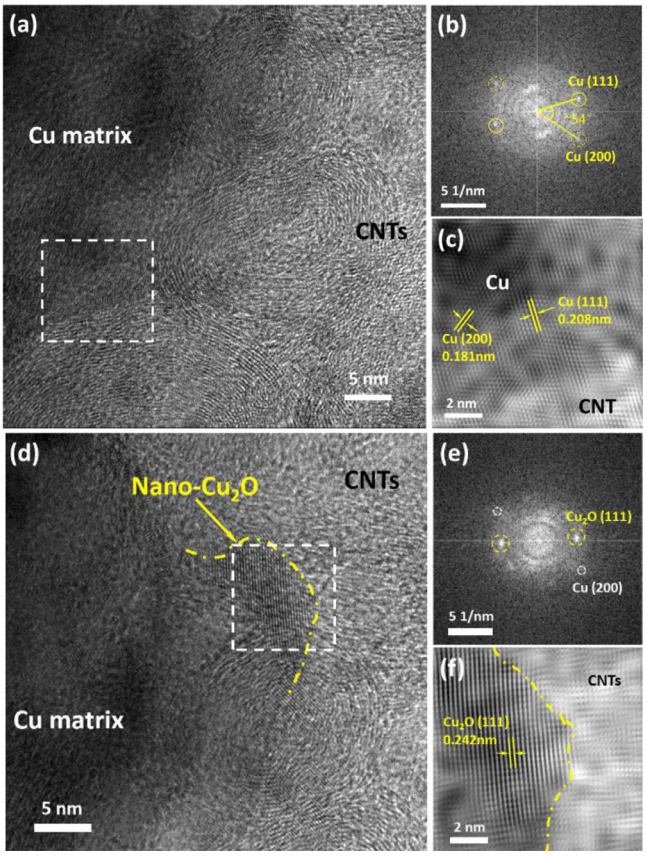

Fig. 1. CNT-Cu interface (a) HRTEM images (b) FFT and (c) inverse FFT of the white box in (a); CNT-Cu_2O interface (d) HRTEM images (e) FFT and (f) inverse FFT of the white box in (d).

3. Results and discussion

3.1. Interface structure from experiment

The interface structure of CNT/Cu composite is studied, as shown in Fig. 1. In Fig. 1a and d, good interfacial adhesion without voids and cracks between the CNT and Cu matrix is observed by HRTEM. To confirm the phases and their relationship, the selected regions of the interface structure of the Fig. 1a and d are carefully

analyzed by corresponding Fast Fourier Transform (FFT) and Inverse Fast Fourier Transform (IFFT). The FFT (Fig. 1b) recorded from the marked box in Fig. 1a shows (111) and (200) diffraction spots of Cu along the [01–1] zone axis. The corresponding IFFT image (Fig. 1c) depicts the clear lattice fringes with the measured inter-planar spacing of 0.208 nm and 0.181 nm, which correspond to the plane of Cu (111) and Cu (200), respectively. Hence, the interfacial layer can be determined to be the Cu and CNT. In another interface area, as shown in Fig. 1e and f, similarly, the FFT shows (111) diffraction spots of Cu_2O and the corresponding IFFT image depicts the clear lattice fringes with the measured inter-planar spacing of 0.242 nm, which correspond to the plane of Cu_2O (111). Thus, this phase at the interface can be determined to be the cubic Cu_2O (Pn3m space group). The results about Cu_2O formation at the Cu/C interface have been reported in several literature [26–29], but the reason for the local formation is still unclear. This may be caused by decomposition of the oxygen-contained functional groups, or oxidation atmosphere and environment, or the insufficient reduction during the preparation process.

3.2. Interface structure of modeling

Because the TEM analysis does not atomistic details of the interface structure, accurate DFT calculations are performed to better understand the micro structure of the Cu/C interface. Based on the above TEM analysis results, we infer that a reasonable interface relationship between Cu and Cu_2O is Cu (111)//Cu_2O (111) in the CNT/Cu composites, which is ascribed by the in-situ oxidation of Cu (111) surface by pyrolysis and diffuse of the oxygen atoms from local oxygen-rich environment or oxygen-contained atmosphere to the sp^2 carbon surface [27]. This relationship is also consistent with the result of visualizing the Cu/Cu_2O interface transition in nanoparticles with environmental scanning transmission electron microscopy in an earlier study [29], which prove that the oxidation occurs via the nucleation of the oxide phase (Cu_2O) from one area of the nanoparticle then progresses unidirectionally across the particle, with the Cu-to-Cu_2O interface having a relationship of Cu (111)//Cu_2O (111). Besides, Cu (111) is the most stable surface facet with the lowest surface energy of 1.34 J/m^2, which is in line with our powder metallurgy process characteristics from powder as raw material [30].

In addition, to simplify the computational model, GR structure was adoped to represent sp^2-C, because the CNT material employed in our experiments has enough large diameters (30–80 nm), which has a similar carbon six-membered ring skeleton to the graphene. A range of interfaces have been considered in this paper, including Cu (111)//GR (001), Cu_2O(111)//GR (001), Cu(111)//Cu_2O (111) and Cu(111)//Cu_2O(111)//GR (001) (see Fig. S1).

3.2.1. Construction of lattice-matched interface structure

To construct lattice-matched interface structures, we first optimized the lattice parameters of bulk Cu, Cu_2O and graphite solids, then obtained the equilibrium lattice parameters of $a = 3.637$ Å; $a = 4.276$ Å and $a = 2.464$ Å, $c = 6.802$ Å for face-centered cubic Cu, body-centered cubic Cu_2O and graphite, respectively, the errors are within 0.6%, 0.2% and 1.4% in comparison with the experimental value, respectively. Then we constructed slab supercell models for Cu and Cu_2O using the crystal lattice parameters, which were laterally co-periodic to the graphene with lattice mismatch less than 5.0% (Lattice mismatch is defined as $(a_1–a_2)/a_1$. see Table 1 for details). The model of Cu/Cu_2O interface was established by the same method and principle. The Cu (111), Cu_2O (111) and GR (001) surfaces were taken for calculating the mismatch of the interfaces. The Cu_2O (111) slab is formed by a succession of O–Cu–O tri-layers, ending with a (stoichiometric, non-polar) oxygen termination [31].

In the interface model, the simulation supercell includes a slab of four-layer Cu, three-layer graphene, three O–Cu–O layers Cu_2O, and a vacuum region of 30 Å thick along z axis. Note that multilayer GR was used instead of monolayer GR to ensure the 'bulk like' electronic behavior at the GR side of the interfaces. The number of atoms in each interface model is 40, 222 and 358, respectively, and the detail is shown in the Table 1. The Brillouin-Zone (BZ) integration is performed using Gamma-centered k-grid of $(6 \times 6 \times 1)$ $(2 \times 2 \times 1)$ and $(1 \times 1 \times 1)$ for Cu/GR, Cu_2O/GR and Cu/Cu_2O, respectively.

The lattice parameters of Cu as a matching reference for building Cu/Cu_2O and Cu/GR; Cu_2O as a matching reference for Cu_2O/GR, and slightly compress the graphene lattice to compensate the mismatch.

3.2.2. Interface geometry

Initially, the optimal configurations of Cu/GR, Cu_2O/GR and Cu/Cu_2O were carefully determined after a series of single-point energy calculations by gradually shifting the relative positions of one material with respect to another along lattice vector $\boldsymbol{a}$ and $\boldsymbol{b}$, and the configurations with the lowest single-point energies of each interface were chosen for further geometry relaxations. For Cu/GR interface, we tried to move the relative positions between Cu slab and graphene, and five different configurations were obtained (see Fig. S2). By calculating the single point energies (in Fig. S3), for our analysis, we only focus on the most stable one, but it is likely that other configurations with slightly higher energies may be observed as well, which corresponds to the top-site carbon located directly above the metallic atom and the hollow-site carbon placed at the hollow site. Similarly, we obtained optimized configuration of Cu_2O/GR and Cu/Cu_2O interface (Figs. S4 and S7). Then, based on these most stable configurations, the interfaces were optimized. The interface structural parameters before and after optimization are listed in (Tables S1–S3). Fig. 2 shows the optimal configuration of the Cu/GR, Cu_2O/GR and Cu/Cu_2O interface, respectively.

Table 2 gives the DFT calculated results of the interfaces. The strength of the interface interactions can be characterized by the binding energy defined as:

$$\boldsymbol{E_b} = \left(\boldsymbol{E_{interface\left(\frac{A}{B}\right)}} - \boldsymbol{E_{slab(A)}} - \boldsymbol{E_{slab(B)}}\right)/\mathbf{s} \quad (1)$$

where $\boldsymbol{E_{interface\left(\frac{A}{B}\right)}}$, $\boldsymbol{E_{slab(A)}}$ and $\boldsymbol{E_{slab(B)}}$ are the energies of the interfaces, ***slab(A)*** and ***slab(B)*** in the optimized interface geometry, respectively; $\boldsymbol{s}$ denotes the area of the interface in the optimal configuration. Negative binding energies indicate the formation of these interfaces is energetically favorable.

The average distances ($\boldsymbol{d_z}$ values defined as the difference between average Z coordinates of the two layers of atoms at the interface) of Cu/GR, Cu_2O/GR and Cu/Cu_2O interfaces are 3.1 Å, 2.7 Å and 1.8 Å, respectively. For Cu_2O/GR, the average distance is ~2.67 Å with full relaxation, which is in good agreement with previous literature [32]. Once Cu_2O is formed, the distance between the slabs are shortened from 3.1 Å to 2.25 Å. The interface binding energies of them are −0.616 J/m^2, −0.471 J/m^2 and −2.623 J/m^2, respectively. The interfacial energies are decreased after the formation of the Cu_2O precipitate. By comparing the equilibrium distances and interface binding energies of the three interfaces, we find that Cu/Cu_2O interface has the strongest interaction between two slabs with the equilibrium average distance of 1.80 Å and the binding energy of −2.623 J/m^2.

3.3. Interface structure

3.3.1. Cu/GR interface

To reflect all the intrinsic interface effect, including the chemical composition, structural distortion, orientation and strain in

Table 1
Parameters of the building interfaces.

Types	Cu/GR			Cu_2O/GR			Cu/Cu_2O		
Supercell size	1 × 1/2 × 2	2 × 2/2 × 2	2 × 2/1 × 1	2 × 2/4 × 4	2 × 2/5 × 5	2 × 2/6 × 6	6 × 6/3 × 3	7 × 7/3 × 3	8 × 8/3 × 3
Mismatch%	−93.6	**3.2**	35.5	18.5	**−1.9**	−22.2	−18.8	**−1.8**	10.9
Atoms number	Cu 16 C 24			Cu 48 O 24 C 150			Cu 196 Cu 108 O 54		
k-grid	6 × 6 × 1			2 × 2 × 1			1 × 1 × 1		

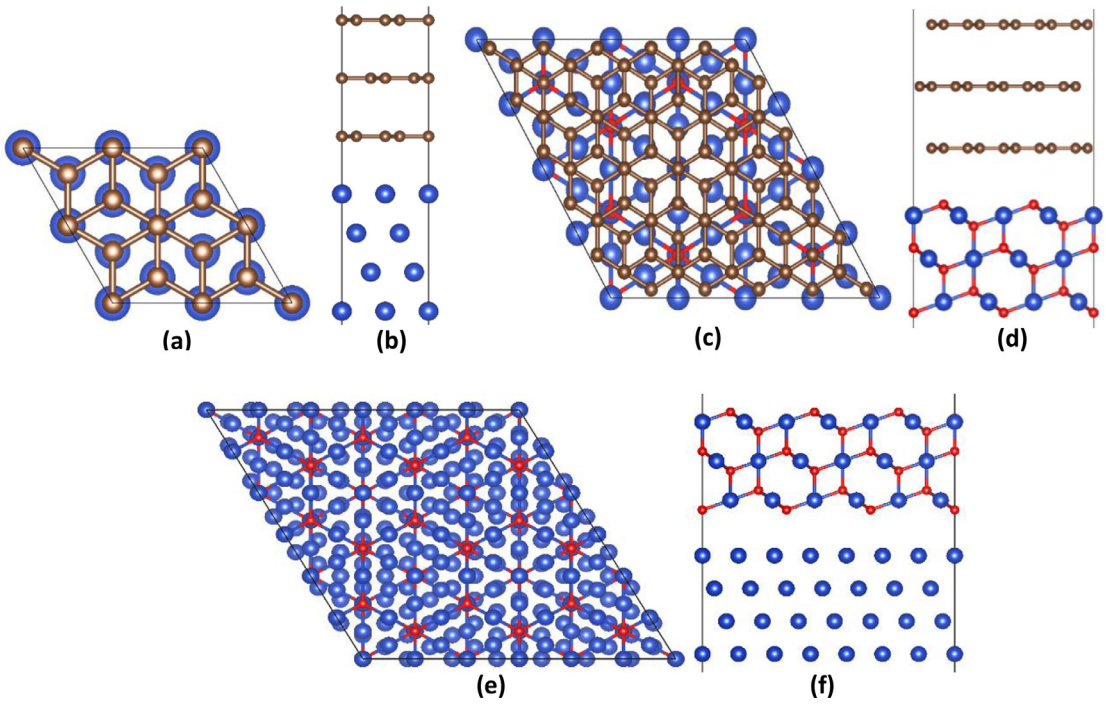

Fig. 2. Optimal configuration of Cu/GR, Cu_2O/GR and Cu/Cu_2O interface with minimal energy, respectively. (a, c, e) Top view and (b, d, f) side view. (Cu, O and C atoms are represented by blue, red and gray balls, respectively.)

Table 2
DFT calculated results of the interfaces, equilibrium average distance d_z and binding energy E_b.

Type	Cu/GR	Cu_2O/GR	Cu/Cu_2O
d_z (Å)	3.10	2. 70 Average: 2.25	1.80
E_b (J/m^2)	−0.616	−0.471 Average: −1.547	−2.623

the potential, a supercell calculation of Cu/GR, Cu substrate and GR slab are carried out in which the planar microscopic potential along the direction perpendicular to the interface (z axis) is calculated in by averaging the Hartree potentials in the plane parallel to the interface (see Figs. 3(a) and S4), then the reference was chosen as the self-consistent electrostatic potential in the vacuum. Owing on the surface reconstruction and interface interaction, the calculated work function (w_f) of the interface is ~4.42 eV while the GR slab is ~4.34 eV and Cu substrate is ~4.91 eV, indicating that the formation of an interface will decrease the resistance of electron transfer from Cu substrate at the Cu/GR interface, but increase the difficulty of that from GR to the interface. Namely, once Cu/C interface is formed, the transfer of the electron becomes more easily than in the pure Cu substrate.

Bader's "atoms-in-molecules" approach is physically intuitive and is firmly based on a quantum mechanical observable electron density. Bader's method has been served to determine atomic partial charges in the constructed interface, the results are illustrated in Figs. 3a and S4. Calculations yield the total electron transfer of $\boldsymbol{Q} = 0.096e$ from the Cu (111) substrate to the GR slab. The amount of microscale charge transfer shows that the interaction between the Cu (111) and GR slab is very weak, which is consistent with the calculated binding energy of -0.616 J/m^2. A few electrons are still transferred from Cu side to the GR, which may be related to the fact that transition metal d-orbitals are usually very diffused (i.e. long tail), and when the charge density near a C atom is integrated, part of that electron density associated with Cu is counted towards C, but this is not a true reflection of the electron transfer. Another reason may be that Cu does not have empty d-orbitals, which is very different when the Cu atoms are replaced with Ni atoms. Hence, considering the weak charge transfer, we believe that the probability of electron transfer at the interface is very small and therefore can be ignored. The electron transport on graphene layer is much larger than that between the layers due to the conjugation of π bond and 2D microstructure. To visualize the Cu/GR interaction, the electron density differences with respect to isolated Cu and GR slabs are present in Fig. 3b. Charge redistribution mainly occurs at the interfacial region between the first GR and Cu (111) atom layer, in which the gap states emerge mainly in the interface area and not penetrate deeply into the 'bulk' region, which is also consistent with the longer distance between the two slabs calculated previously.

3.3.2. Cu_2O/GR interface

Planar-averaged local potentials for the Cu_2O/GR interface, GR slab and Cu_2O slab is given in Figs. 4a and S7. The calculated w_f of Cu_2O (111) slab is ~5.14 eV, and that of GR slab is ~4.03 eV. Unlike the Cu/GR interface, both of the w_f of Cu_2O slab and GR

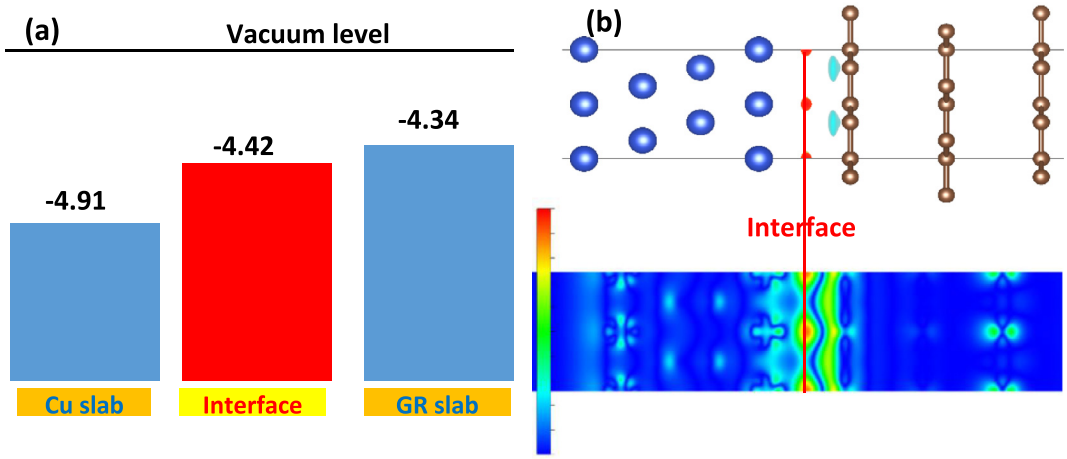

Fig. 3. (a) Work function of the Cu/GR interface and slabs; (b) Electronic density difference plot of interface structure, showing charge transfer in the region between the surface of graphene and copper atoms. Isosurface value for the structures is 0.0004 e/Å^3, where the accumulation and depletion of electrons are indicated in yellow and green, respectively. (Cu, and C atoms are represented by blue and gray balls, respectively.)

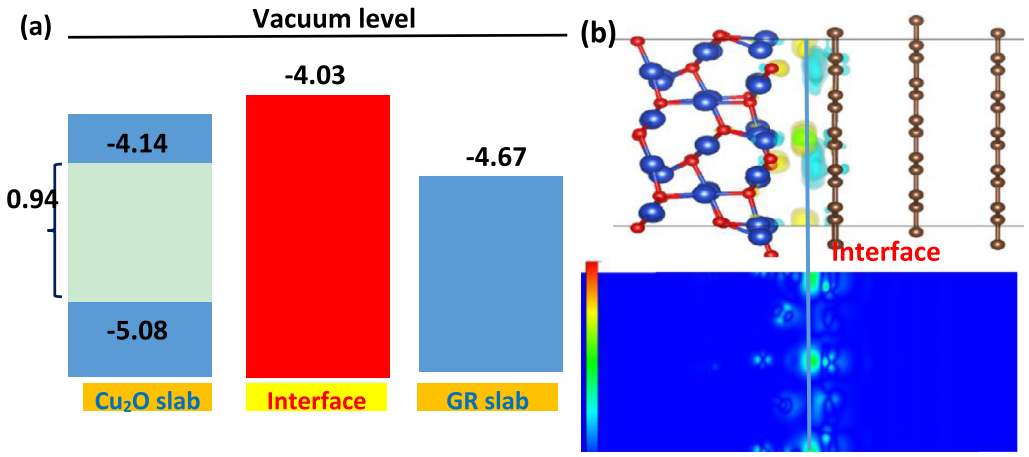

Fig. 4. (a) Work functions and Bader charges of the Cu_2O/GR interface and slabs; (b) Electronic density difference plot of interface structure, showing charge transfer in the region between the surface of graphene and copper atoms. Isosurface value for the structures is 0.0004 e/Å^3, where the accumulation and depletion of electrons are indicated in yellow and green, respectively. (Cu, O and C atoms are represented by blue, red and gray balls, respectively.)

part are decreased significantly from 5.08 eV to 4.03 eV, and from 4.67 eV to 4.03 eV respectively after the interface is generated. Obviously, the interface interaction of the Cu_2O and GR will decrease the work function. The distribution of Bader charges of the Cu_2O/GR interface with the *z*-axis (see Fig. S10) proves that the total electron transfer of Q_{tot} from the GR slab to the Cu_2O (111) substrate is ~0.231e, which is much larger than that of Cu/GR interface, suggesting that the interaction between the Cu_2O (111) and graphene slab is much stronger. The Bader charges of each carbon atom in the GR slab is +0.001e. Fig. 4b gives the electronic density difference plot of interface structure, showing the interfacial charges transfer from GR to Cu_2O slab, and the partial atomic charges on the surface of the Cu_2O (111) substrate is increased.

3.3.3. *Cu/Cu$_2$O interface*

Very different from the Cu_2O/GR interface, once the Cu/Cu_2O interface is generated, the w_f of the Cu substrate will be increased from 5.01 eV to 5.22 eV but that of the Cu_2O part is reduced from 5.46 eV to 5.22 eV. This indicates that the formation of interface is beneficial for the transfer of electrons in Cu_2O slab, but the electron transfer become harder in the Cu substrate. The distribution of Bader charges of the Cu/Cu_2O interface shows that the total electron transfer of Q_{tot} from the Cu substrate to the Cu_2O (111) is ~3.042 e per simulation cell in Fig. S10. The Bader charge of each Cu atom in the Cu slab is +0.016e, which is the largest value of the three interfaces, indicating that the interaction between the Cu_2O (111) and Cu (111) slab is the strongest. Fig. 5b gives the electronic density difference plot of interface structure, showing the interfacial charges transfer from Cu to Cu_2O slab.

3.3.4. *Cu/Cu$_2$O/GR interface*

Fig. 6(a,b) shows the optimized structure of the Cu/Cu_2O/GR interface from the top and side view. Fig. 6(c) gives the distribution of Bader charges of the Cu/Cu_2O/GR interface with *z*-axis. The total charge transfer mainly occurs at the interface between Cu and Cu_2O, while the charge transfer at the interface between GR and Cu can be ignored. This not only indicates that there is a strong chemical bond between Cu and Cu_2O interface, but also that transferred electrons are localized on the oxygen ions. Fig. 6(d) shows the w_f of the Cu/Cu_2O/GR interfaces. The w_f of the graphene shows a larger amplitude than that of Cu and Cu_2O, which means the excellent electronic transport characteristics in the plane. Besides, there is a significant increase in w_f at the Cu/Cu_2O and Cu_2O/GR interface owing to the Schottky barrier. As known, Schottky barrier height, which is a key parameter for the interfacial electrical characteristics, can be formed in a metal-semiconductor interface due to the difference of the work function. Hence, Schottky contact with a high barrier means a big contact resistance,

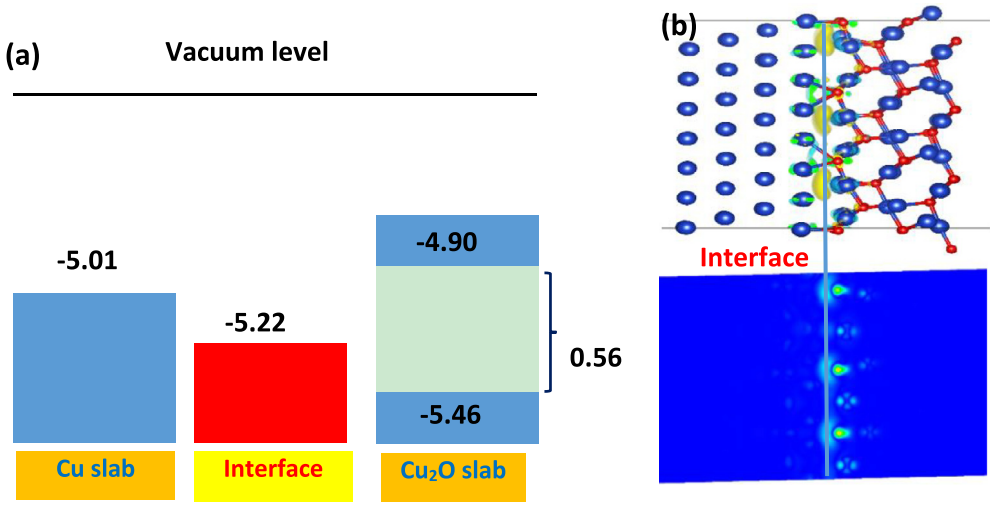

Fig. 5. (a) Work functions and Bader charges of the Cu/Cu_2O interface and slabs; (b) Electronic density difference plot of interface structure, showing charge transfer in the region between the surface of graphene and copper atoms. Isosurface value for the structures is 0.0004 e/Å^3, where the accumulation and depletion of electrons are indicated in yellow and green, respectively. (Cu, O and C atoms are represented by blue, red and gray balls, respectively.)

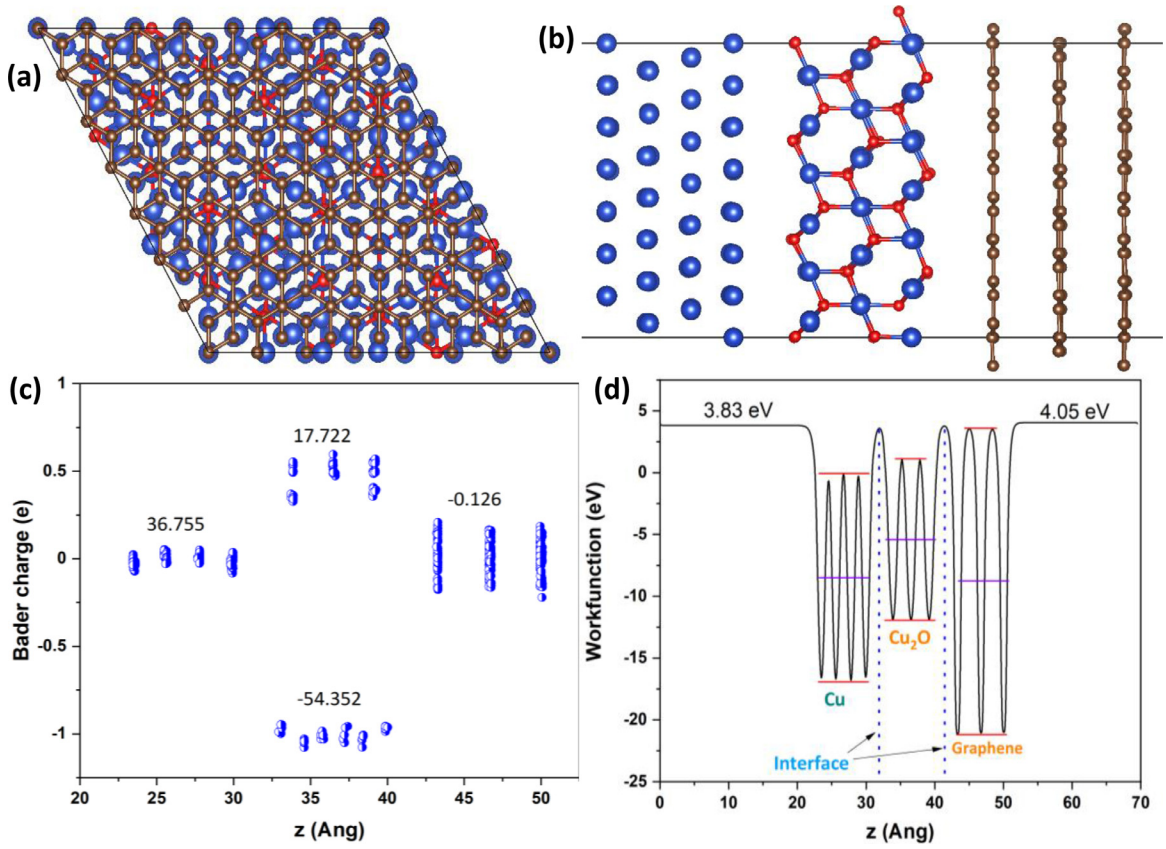

Fig. 6. (a) Top and (b) side view of the optimized structure of the Cu/Cu_2O/GR interface (The red balls for O atoms, the blue balls for Cu atoms and the dark gray balls for C atoms). (c) Distribution of Bader charges and (d) Work function of the interface with the *z*-axis. (Cu, O and C atoms are represented by blue, red and gray balls, respectively.)

thus more power loss in the interfacial region. This is also proving that once Schottky barrier is formed, the charge will gather at the interface, which makes the electron migration more difficult. In addition, we find that the difficulty of the electron transfer from GR to Cu_2O is much higher than that from Cu to Cu_2O. Since the conductivity of a material is governed by both the mean free path length and the electron density of state, electronic DOS distributions in the three interfaces were calculated as shown in Fig. S11. As expected, no band-gap and d-states cross the fermi level with nonmagnetic states on the Cu atoms are found. Due to the 2D structure and π conjugation of graphene, the DOS of the Cu-GR and Cu_2O-GR interfaces are weak. This is consistent with the weak physical adsorption between GR and 'O' determinate surface of Cu_2O. Moreover, the Cu–Cu_2O interface shows a DOS peak at Fermi level which means that there is a contribution from the overlap between Cu_2O and Cu substrates.

4. Conclusion

Based on the experimental results and simulation analysis, we conclude that the formation of the Cu_2O at the Cu/GR interface will reduce the total equilibrium average distance from 3.10 to 2.25 Å but increase the binding energy of the two slabs, both of them beneficial to enhance the mechanical property of the composites. However, Schottky barrier will be introduced into the interface of Cu/Cu_2O, which will make the transferred electrons accumulate at the interface and increase the difficulty of electron migration. From this point of view, when the quantity of the Cu_2O reaches an order of magnitude with the average free path of electrons, the conductivity of the composites will be affected intensively. Besides, the electron transfer at the interface between Cu and GR is very weak. Although the appearance of Cu_2O can improve the electron transport between Cu_2O and Cu, there is still a problem of difficult charge transfer between Cu_2O and GR. Hence, this study will provide a way to improve the interface properties of the Cu/sp^2-carbon composite by controlling the formation and distribution states.

Declaration of Competing Interest

The authors declare that they have no known competing financial interests or personal relationships that could have appeared to influence the work reported in this paper.

Acknowledgments

This work is supported by the Chinese National Natural Science Foundation (Grant no. 52064032), the Yunnan Science and Technology projects (Grant nod. 2019ZE001 and 202002AB080001), Yunnan Ten Thousand Talents Plan Young & Elite Talents Project (YNWR-QNBJ-2018-005). We acknowledge the use of the Athena supercomputer through the HPC Midlands+ Consortium, and the ARCHER supercomputer through membership of the UK's HPC Materials Chemistry Consortium, which are funded by EPSRC Grants No. EP/P020232/1 and No. EP/R029431/1, respectively. We would also like to acknowledge the support from Propulsion Futures Beacon project, The University of Nottingham.

Supplementary materials

Supplementary material associated with this article can be found, in the online version, at doi:10.1016/j.cartre.2021.100046.

References

[1] D. Kong, Z. Xiao, Y. Gao, X. Zhang, R. Guo, X. Huang, X. Li, L. Zhi, Sp2-carbon dominant carbonaceous materials for energy conversion and storage, Mater. Sci. Eng. R Rep. 137 (2019) 1–37, doi:10.1016/j.mser.2018.10.001.
[2] M.J. Allen, V.C. Tung, R.B. Kaner, Honeycomb carbon: a review of graphene, Chem. Rev. 110 (1) (2010) 132–145, doi:10.1021/cr900070d.
[3] R.J. Young, I.A. Kinloch, L. Gong, K.S. Novoselov, The mechanics of graphene nanocomposites: a review, Compos. Sci. Technol. 72 (12) (2012) 1459–1476, doi:10.1016/j.compscitech.2012.05.005.
[4] W. Choi, I. Lahiri, R. Seelaboyina, Y.S. Kang, Synthesis of graphene and its applications: a review, Crit. Rev. Solid State Mater. Sci. 35 (1) (2010) 52–71, doi:10.1080/10408430903505036.
[5] W.A.D.M. Jayathilaka, A. Chinnappan, S Ramakrishna, A review of properties influencing the conductivity of CNT/Cu composites and their applications in wearable/flexible electronics, J. Mater. Chem. C 5 (36) (2017) 9209–9237, doi:10.1039/C7TC02965A.
[6] S.R. Bakshi, D. Lahiri, A. Agarwal, Carbon nanotube reinforced metal matrix composites-a review, Int. Mater. Rev. 55 (1) (2010) 41–64, doi:10.1179/095066009X12572530170543.
[7] I. Tajzad, E. Ghasali, Production methods of CNT-reinforced Al matrix composites: a review, J. Compos. Compd. 2 (1) (2020) 1–9, doi:10.29252/jcc.2.1.1.
[8] B.V. Ramnath, C. Parswajinan, C. Elanchezhian, S.V. Pragadeesh, P.R. Ramkishore, V. Sabarish, A review on CNT reinforced aluminium and magnesium matrix composites, in: Applied Mechanics and Materials, 591, Trans Tech Publications Ltd, 2014, pp. 120–123. 10.4028/www.scientific.net/AMM.591.120.
[9] M. Alishahi, S.M. Monirvaghefi, A. Saatchi, S.M. Hosseini, The effect of carbon nanotubes on the corrosion and tribological behavior of electroless Ni–P–CNT composite coating, Appl. Surf. Sci. 258 (7) (2012) 2439–2446, doi:10.1016/j.apsusc.2011.10.067.
[10] G.A. López, E.J. Mittemeijer, The solubility of C in solid Cu, Scr. Mater. 51 (1) (2004) 1–5, doi:10.1016/j.scriptamat.2004.03.028.
[11] X. Liu, Y. Liu, X. Ran, et al., Fabrication of the supersaturated solid solution of carbon in copper by mechanical alloying, Mater. Charact. 58 (6) (2007) 504–508, doi:10.1016/j.matchar.2006.06.022.
[12] X. Mi, V. Meunier, N. Koratkar, et al., Facet-insensitive graphene growth on copper, Phys. Rev. B 85 (15) (2012) 155436, doi:10.1103/PhysRevB.85.155436.
[13] X. Chen, J. Tao, J. Yi, Y. Liu, C. Li, R. Bao, Strengthening behavior of carbon nanotube-graphene hybrids in copper matrix composites, Mater. Sci. Eng. A 718 (2018) 427–436, doi:10.1016/j.msea.2018.02.006.
[14] B. Cheng, R. Bao, J. Yi, C. Li, J. Tao, Y. Liu, S. Tan, X. You, Interface optimization of CNT/Cu composite by forming TiC nanoprecipitation and low interface energy structure via spark plasma sintering, J. Alloys Compd. 722 (2017) 852–858, doi:10.1016/j.jallcom.2017.06.186.
[15] K. Chu, C.C. Jia, L.K. Jiang, W.S. Li, Improvement of interface and mechanical properties in carbon nanotube reinforced Cu–Cr matrix composites, Mater. Des. 45 (2013) 407–411, doi:10.1016/j.matdes.2012.09.027.
[16] K. Chu, F. Wang, Y.B. Li, X.H. Wang, D.J. Huang, Z.R. Geng, Interface and mechanical/thermal properties of graphene/copper composite with Mo_2C nanoparticles grown on graphene, Compos. Part A 109 (2018) 267–279, doi:10.1016/j.compositesa.2018.03.014.
[17] Q.H. Yuan, G.H. Zhou, L. Liao, Y. Liu, L. Luo, Interfacial structure in AZ91 alloy composites reinforced by graphene nanosheets, Carbon 127 (2018) 177–186, doi:10.1016/j.carbon.2017.10.090.
[18] K. Chu, J. Wang, Y.P. Liu, Z.R. Geng, Graphene defect engineering for optimizing the interface and mechanical properties of graphene/copper composites, Carbon 140 (2018) 112–123, doi:10.1016/j.carbon.2018.08.004.
[19] P.G. Koppad, H.A. Ram, C.S. Ramesh, K.T. Kashyap, R.G. Koppad, On thermal and electrical properties of multiwalled carbon nanotubes/copper matrix nanocomposites, J. Alloys Compd. 580 (2013) 527–532, doi:10.1016/j.jallcom.2013.06.123.
[20] S. Stankovich, D.A. Dikin, G.H. Dommett, K.M. Kohlhaas, E.J. Zimney, E.A. Stach, R.D. Piner, S.T. Nguyen, R.S. Ruoff, Graphene-based composite materials, Nature 442 (7100) (2006) 282–286, doi:10.1038/nature04969.
[21] S. Ling, M.B. Watkins, A.L. Shluger, Effects of oxide roughness at metal oxide interface: MgO on Ag (001), J. Phys. Chem. C 117 (10) (2013) 5075–5083, doi:10.1021/jp311141k.
[22] S. Ling, M.B. Watkins, A.L. Shluger, Effects of atomic scale roughness at metal/insulator interfaces on metal work function, PCCP 15 (45) (2013) 19615–19624, doi:10.1039/C3CP53590H.
[23] J. Moellmann, S. Grimme, DFT-D3 study of some molecular crystals, J. Phys. Chem. C 118 (14) (2014) 7615–7621, doi:10.1021/jp501237c.
[24] A.K. Mishra, A. Roldan, N.H. de Leeuw, A density functional theory study of the adsorption behaviour of CO_2 on Cu_2O surfaces, J. Chem. Phys. 145 (4) (2016) 044709, doi:10.1063/1.4958804.
[25] K. Momma, F. Izumi, VESTA 3 for three-dimensional visualization of crystal, volumetric and morphology data, J. Appl. Crystallogr. 44 (6) (2011) 1272–1276, doi:10.1107/S0021889811038970.
[26] X. Chen, J. Tao, Y. Liu, R. Bao, F. Li, C. Li, J. Yi, Interface interaction and synergistic strengthening behavior in pure copper matrix composites reinforced with functionalized carbon nanotube-graphene hybrids, Carbon 146 (2019) 736–755, doi:10.1016/j.carbon.2019.02.048.
[27] X. Chen, R. Bao, J. Yi, D. Fang, J. Tao, Y. Liu, Enhancing interfacial bonding and tensile strength in CNT-Cu composites by a synergetic method of spraying pyrolysis and flake powder metallurgy, Materials 12 (4) (2019) 670, doi:10.3390/ma12040670.
[28] X. Lian, P. Xiao, R. Liu, G. Henkelman, Calculations of oxygen adsorption-induced surface reconstruction and oxide formation on Cu (100), Chem. Mater. 29 (4) (2017) 1472–1484, doi:10.1021/acs.chemmater.6b02722.
[29] A.P. LaGrow, M.R. Ward, D.C. Lloyd, P.L. Gai, E.D. Boyes, Visualizing the Cu/Cu_2O interface transition in nanoparticles with environmental scanning transmission electron microscopy, J. Am. Chem. Soc. 139 (1) (2017) 179–185, doi:10.1021/jacs.6b08842.
[30] R. Tran, Z. Xu, B. Radhakrishnan, D. Winston, W. Sun, K.A. Persson, S.P. Ong, Surface energies of elemental crystals, Sci. Data 3 (1) (2016) 1–13, doi:10.1038/sdata.2016.80.
[31] C. Gattinoni, A. Michaelides, Atomistic details of oxide surfaces and surface oxidation: the example of copper and its oxides, Surf. Sci. Rep. 70 (3) (2015) 424–447, doi:10.1016/j.surfrep.2015.07.001.
[32] K. Cheng, N. Han, Y. Su, J. Zhang, J. Zhao, Schottky barrier at graphene/metal oxide interfaces: insight from first-principles calculations, Sci. Rep. 7 (2017) 41771 (2017), doi:10.1038/srep41771.